# Temperature dependence of ternary solution particle volumes as observed by lidar in the Arctic stratosphere during winter 1992/93

G eorg Beyerle[1,2], Beiping LUO[3,4], Roland Neuber[2], Thomas Peter[4], and
I. Stuart McDermid[1]

Short title:   TERNARY SOLUTION PARTICLE VOLUMES

[1] Jet Propulsion Laboratory, Table Mountain Facility, California Institute o f
Technology, Wrightwood, USA

[2] Alfred Wegener Institute for Polar and Marine Research, Potsdam, Germany

[3] Lehrstuhl für Biokli matologie und Immissionsforschung, Universität München,
Freising, Germany

[4] Max-Planck-Institut für Chemie, Mainz, Germany

Abstract.

Multiwavelength lidar measurements of stratospheric aerosols performed at the Arctic NDSC station 011 Spitsbergen during winter 1992/93 are analyzed. Altitude profiles of particle median radius and volume density are derived for measurements with aerosol depolarization smaller than 0.01. Below an altitude corresponding to 450 K potential temperature the Pinatubo aerosol layer dominated the stratospheric aerosol content with volume densities of more than 10 $\mu m^3/cm^3$ whereas above 450 K volume densities were close to background values of 0.1 $\mu m^3/cm^3$. However, at all altitude levels between 350 and 550 K volume densities consistently increased by a factor of 2-30 when temperatures approached the frost point. The observations are compared to results from thermodynamic model calculations at altitude levels of 400, 440, and 480 K. Good agreement between the observed and theoretically derived temperature dependencies of volume density suggests that type Ib polar stratospheric clouds as well as volcanic aerosols at low temperatures are composed of a ternary liquid solution of sulfuric and nitric acid. At all altitude levels model results indicated more than 90% $HNO_3$ gas phase depletion as temperatures approached the frost point. A mean profile of total $H_2SO_4$ vmr is derived decreasing from about 4 ppbv at 350 K to about *0.5 ppbv* above *450 K,*

# Introduction

Polar stratospheric clouds (PSCs) play a fundamental role in Arctic and Antarctic stratospheric chemistry. Heterogeneous reactions occurring on PSC particle surfaces activate chlorine species leading to catalytic ozone loss. There are two major types of PSCs [*Poole and McCormick*, 1988; *Browell et al., 1990; Toon et al.*, 1990]: type 11 PSCs are observed below the frost point and thought to be water ice clouds, while type 1 PSCs are observed to exist at temperatures 5 7 K above the frost point. The composition and phase of type I PSCs is still uncertain [*Dye et al., 1992*]. Recent analyses of ER-2 in-situ measurements by *Carslaw et al.* [] 994] and *Drdla et al. [1* 994] indicate that some of the observed type 1 PSCs were not composed of nitric acid trihydrate (N AT) but of a ternary liquid solution of $H_2SO_4$, $HNO_3$, and $H_2O$. Furthermore, laboratory measurements have shown that aqueous solutions of sulfuric and nitric acid are unlikely to freeze under stratospheric conditions for temperatures above the frost point [*Koop et al.*, 1995]. Thermodynamic mode] calculations show that water and nitric acid are taken up by the sulfuric acid aerosol if temperatures approach the frost point thereby changing its composition from binary $H_2SO_4$ droplets to ternary solution particles with $H_2SO_4$ weight percentage of less than 5% [*Carslaw et al.,* 1994; *Tabazadeh et al.*, 199'4].

*Dye et al. [1* 992] have analyzed the growth of stratospheric sulfuric acid aerosols using ER-2 in-situ measurements during background conditions in January 1989. At altitudes between 440 and 460 K they found a 50 fold increase in the particle volume density due to $HNO_3$ uptake as temperatures approached the frost point. For another ER-2 flight in 1992 *Toon et al.* [1993] have attributed the observed gas phase depletion of $HNO_3$ to uptake into volcanic $H_2SO_4$ aerosols. In this paper we discuss the temperature dependence of particle volume densities in the presence of volcanic aerosols and directly compare this with the observed aerosol growth at higher, volcanically unperturbed altitudes. The volcanic sulfuric acid aerosols are due to the eruption

of the Philippine volcano Mt. Pinatubo in June 1991 [*McCormick and Veiga*, 1992]. Our analysis is based on lidar measurements of volcanic aerosols and PSCs recorded during winter 1992/93 at the Arctic NDSC (Network for the Detection of Stratospheric Change) station (Koldewey station) in Ny-Ålesund, Spitsbergen (79°N, 12°E) [*Beyerle et al.*, 1994].

After a brief description of the measurement we discuss the derivation of backscatter coefficients and size distributions from the lidar data. Due to the lower spatial and temporal resolution of our remote sensing data compared to in-situ measurements we use a statistical approach in order to derive the temperature dependence of volume density of stratospheric ternary solution (S'1'S) particles from observations recorded over a period of two months in winter 1992/93. Finally the results are compared to S'1'S model calculations.

## Instrumentation and data reduction

Multiwavelength lidar observations of stratospheric aerosols have been performed at Koldewey station since November 1991. During the winter 1992/93 the aerosol lidar system operated at three wavelengths: the Raman shifted wavelength of a XeCl Excimer laser (353 nm) and the fundamental and first harmonic of a Nd:YAG laser (1064 and 532 nm). The laser pulse repetition frequency was 30 Hz with UV- and V] S/1 R- channels triggered alternately in order to reduce cross-talk between detection channels. Additionally, volume depolarization at 532 nm was recorded. Saturation of the photodetectors by intense signals backscattered from the troposphere was prevented by means of a mechanical shutter (chopper). The altitude range between the tropopause (typically between 8 and 10 km at Spitsbergen) and about 40 km was covered with a spatial resolution of 200 In. For data analysis signal counts were integrated over 40,000 laser pulses resulting in a temporal resolution of 22 min. Instrumental details are described by *Neuber et al.* [19!32] and *Beyerle and Neuber* [1994].

## Derivation of backscatter coefficients

The particle backscatter coefficient $\beta^A$ as a function of altitude $z$ is derived using Klett's algorithm with constant ratios of extinction to backscatter coefficient, $L(z) = \alpha^A(z)/\beta^A(z)$ [*Klett*, 1985]. During the winter 1992/93 the lidar system was not yet equipped with a Raman detection channel and therefore the value of the lidar ratio $L = 30$, 40 and 60 sr $\pm$ 50% at 353, 532 and 1064 nm, respectively, is taken from the literature [*Jäger and Hofmann*, 1991; *Thomason and Osborn*, 1992]. Profiles of the molecular backscatter coefficient $\beta^R(z)$ are calculated from temperature and pressure profiles obtained from daily aerological soundings at Koldewey station. The sondes usually reached altitudes of more than 30 km. As no aerosols were observed above 25 km data from model atmospheres are not required. We determine the constant of integration in Klett's algorithm by imposing $\beta^A(z_i) = 0$ m$^{-1}$sr$^{-1}$ in the least square sense for all altitude levels $z_i$ between 25 km and the upper end of the observed density profile [*Klett*, 1985]. The statistical variations of the measured signal counts, which are assumed to follow Poisson statistics, and the uncertainty of the density profile represent the dominating contributions to the error of $\beta^A(z)$. Typically, the relative errors of $\beta^A(z, \lambda = 353, 532$ nm) are 5 10% and for $\beta^A(z, \lambda = 1064$ nm) are 20- 30% at altitudes between 10 and 20 km.

## Derivation of size distributions

From the wavelength dependence of the particle backscatter coefficients $\beta^A(\lambda_i)$ ($\lambda_1 = 353$ nm, $\lambda_2 = 532$ nm, and $\lambda_3 = 1064$ nm) information on the particle size distribution) is extracted. The extinction coefficients $\alpha^A = L\beta^A$ are not taken into account because of the large systematic uncertainty of the lidar ratio $L$. Our procedure is based on algorithms described by *Larsen* [1992] and *Beyerle et al.* [1994]. As the measurements provide only three pieces of information on the actual size distribution we restrict the number of possible solutions of the inversion problem by imposing the

following constraints:

1. The aerosol size distribution is assumed to be a monomodal lognormal distribution [*Pinnick et al.*, 1976]

$$\frac{dN^A}{dr} = \frac{\mathcal{N}^A}{\sqrt{2\pi}\, r\, \ln(s)} \exp\left(-\frac{\ln^2(r/\tilde{r})}{2\ln^2 s}\right) , \tag{1}$$

where $\mathcal{N}^A$, $\tilde{r}$ and s denote the particle number density, the median radius and the geometric standard deviation, respectively.

2. The particle number density is constant, $\mathcal{N}^A = 15\ \mathrm{cm}^{-3}$.

3. The particles are composed of an aqueous solution of nitric and sulfuric acid in thermodynamic equilibrium with ambient $HNO_3$ and $H_2O$ vapor.

The validity of the first and second assumption is substantiated by in-situ measurements of the aged Pinatubo aerosol by *Deshler* [1994]. His measurements during January/February 1992 show that the actual size distribution is reasonably well approximated by Eq. 1. Furthermore, condensation nuclei number densities in the altitude range 10 30 km vary only between 5 and 50 cm⁻ 3. As will be discussed later the derived volume densities depend only weakly on the selected value of $\mathcal{N}^A$ provided $5\ \mathrm{cm}^{-3} \lesssim \mathcal{N}^A \lesssim 50\ \mathrm{cm}^{-3}$. The third assumption implies a homogeneous particle composition and a spherical particle shape. Therefore, Mie scattering theory can be used for the size distribution calculation. The assumption is justified by observational and theoretical results [e.g. *Drdla et al.*, 1994; *Carslaw et al.*, 1994] provided there are no rapid temperature fluctuations which could lead to strongly perturbed non-equilibrium compositions [*Meilinger et al.*, 1995].

However, our depolarization measurements indicate that a considerable fraction of the observed aerosols were non-spherical [*Beyerle et al.*, 1994]. Therefore, all measurements with aerosol depolarization $\delta_A = \beta^A_\perp/\beta^A_\parallel$ larger than 0.01 are excluded from the following analysis. Here, $\beta^A_\perp$ $\left(\beta^A_\parallel\right)$ denotes the aerosol backscatter coefficient

derived from the cross-polarization (aligned-polarization) detection channel. We note that due to normalization uncertainties $\delta_A$ is affected by a systematic error of about 50%. The excluded data represent 32% of all measurements with backscatter ratio $R = \beta^A/\beta^R + 1$ at 532 nm larger than 1.1.

The size distribution parameters $\bar{r}$ and s are determined by comparing the measured backscatter coefficients with results from Mie scattering calculations. The median radius $\bar{r}$ and geometric standard deviation s are found by minimizing

$$\chi^2 = \frac{1}{3} \sum_{i=1}^{3} \left( \frac{\beta^A(\lambda_i, z, t) - b(\lambda_i, m)}{\sigma_\beta^A(\lambda_i, z, t)} \right)^2 \tag{2}$$

for every measurement $\beta^A(\lambda_i, z, t)$ at altitude $z$ and time $t$. Here, $\sigma_\beta^A$ denotes the error of $\beta^A(\lambda_i, 2, t)$. The calculated backscatter coefficients $b(\lambda, m)$ are given by

$$b(\lambda, m) = \int_0^\infty dr \, \frac{dN^A}{dr}(r, \mathcal{N}^A, \bar{r}, s) \, \pi \, r^2 \, Q_b\left(\frac{2\pi r}{\lambda}, m\right) . \tag{3}$$

where $Q_b$ is the Mie backscattering efficiency at wavelength $\lambda$ for a spherical particle with radius $r$ and refractive index $m$. $Q_b$ is calculated numerically [Bohren and Huffman, 1983].

As $\chi^2$ depends nonlinearly on $\bar{r}$ and s we determine the global minimum of $\chi^2$ by evaluating Eq. 3 at 142 values of $\bar{r}$ ranging from 0.005 pm to 5.0 $\mu$m with logarithmic steps of 1.05 and 39 values of s ranging from 1.1 to 3 with linear steps of 0.05. If the minimum lies on the border of the $(\bar{r}, s)$-grid (i.e. $\bar{r} = 0.005$ $\mu$m or $\bar{r} = 5$ $\mu$m or $s = 1.1$ or s = 3) the result is rejected.

The procedure is repeated N = 50 times where the measured $\beta^A(\lambda_i, z, t)$ are replaced by $\beta^A(\lambda_i, z, t) + \Delta\beta_j^A$ giving a set of N solutions $\bar{r}_j, s_j, j = 1, \ldots, N$. $\Delta\beta_j^A$ is a Gaussian distributed random value with standard deviation equal to the measurement errors $\sigma_{\beta^A}$. The final values $\bar{r}$ and s are then obtained as geometric means of $\bar{r}_j$ and $s_j$. The volume density $\mathcal{V}$ is calculated from $\mathcal{N}^A$, $\bar{r}$, and s according to the Hatch-Choate equation

$$v = \frac{4}{3} \pi \mathcal{N}^A \bar{r}^3 \exp\left(\frac{9}{2} \ln^2(s)\right) . \tag{4}$$

The covariance matrix $Cov(\hat{r}_j, s_j)$ provides information on the errors of $\hat{r}$ and s, their correlation, and on the error of $\mathcal{V}$.

In order to test the influence of keeping the value of $\mathcal{N}^A$ at 15 cm$^{-3}$ the calculation] was repeated with $\mathcal{N}^A = 5$ cm$^{-3}$ and 50 cm$^{-3}$. On the basis of all 302 profiles the ratios of volume densities $\mathcal{V}(\mathcal{N}^A = 5$ cm$^{-3})/\mathcal{V}(\mathcal{N}^A = 15$ cm$^-$3, and $\mathcal{V}(\mathcal{N}^A = 50$ cm$^{-3})/\mathcal{V}(\mathcal{N}^A = 15$ cm$^{-3})$ are found to be 0.96 and 1.11 with standard deviations of 0.24 and 0.39, respectively. As the relative error of $\mathcal{V}$ is on average 50% choosing $\mathcal{N}^A$ within the range 5 to 50 cm$^{-3}$ does not seem to change the derived volume densities significantly. This result is in accordance with theoretical considerations [e.g. *Heintzenberg et al., 1 981; Thomalla and Quenzel, 1 982*].

Refractive index

Derivation of $\hat{r}$ and s on the basis of Eqs. 2 and 3 requires knowledge of the refractive index $m$ of S'1'S particles which depends on the $H_2SO_4$ and $HNO_3$ weight percentages, $w_S$ and $w_N$. To the best of our knowledge no data on the wavelength and temperature dependence of $m$ as a function of $w_S$ and $w_N$, are currently available. Therefore, $m(\lambda, T, w_S, w_N)$ is calculated based on the 1 orentz-Lorenz relation for the ternary solution. Details of the derivation will be published elsewhere (B. Luo, manuscript in preparation). In the following an altitude independent $H_2O$ vmr of 5 ppmv [*Ovarlez and Ovarlez*, 1994] and an $HNO_3$ vmr profile peaking at 10 ppbv derived from LIMS data is USCd [ *Gille and Russell*, ] 984].

As the total $H_2SO_4$ vmr and, therefore, $w_S$ and $w_N$ are not known a-priori, an iterative procedure is used. (We define total vmr as the volume mixing ratio that would be observed if all molecules in the liquid phase were present in the gas phase. ) First, preliminary volume densities $\tilde{\mathcal{V}}$ are derived using an approximated refractive index $\tilde{m}$. As will be discussed later comparison of $\tilde{\mathcal{V}}$ with S'1'S model results provides an estimate of total $H_2SO_4$ vmr. Finally $w_S$, $w_N$, and $m$ are obtained from the STS model as well

as the Lorentz-Lorenz relation and the size distribution calculation is repeated with $m$.

The approximated refractive index $\tilde{m}$ is obtained in the following way. We assume that the aerosols consist of binary $H_2SO_4/H_2O$ solution in equilibrium with ambient water vapor. Temperature and $H_2O$ partial pressure determine the $H_2SO_4$ weight percentage [*Steele* **and** *Hamill*, 1 981; *Russell and Hamill, 1984*]. From laboratory data by *Palmer and Williams* [1 975] the $H_2SO_4/H_2O$ refractive index at the lidar wavelengths is calculated by inter- and extrapolation. Provided the molar refraction is independent of temperature the refractive index can be corrected for stratospheric temperatures by means of the Lorentz-Lorenz relation

$$\tilde{m}(T) = \sqrt{\frac{1 + 2a}{1 - a}}$$

$$a = \frac{\rho(T)}{\rho(T_0)} \frac{\tilde{m}^2(T_0) - 1}{\tilde{m}^2(T_0) + 2}.$$

where $\rho(T_0)$ denotes the density at laboratory temperature $T_0 = 300$ K. Here, $\tilde{m}$ and $m$ are assumed to be real at the lidar wavelengths.



We note that use of $m$ instead of $\tilde{m}$ modifies the calculated volume densities on average by a factor of 0.S7 ± 0.2. Even if $\tilde{m}$ instead of $m$ was used the conclusion reached in this paper would be the same.

The temperature and wavelength dependence of $m$ is shown in Figure 1 (bottom) using $H_2SO_4$, $HNO_3$, $H_2O$ total vmr of 0.5 ppbv, 10 ppbv and 5 ppmv, respectively. Atmospheric pressure is taken to be 50 hPa. The frost point and the NAT equilibrium temperature are indicated by vertical arrows. The NAT equilibrium temperature is calculated assuming 5 ppmv $H_2O$ and an $HNO_3$ profile peaking at 10 ppbv as derived from LIMS data [*Gille and Russell*, 1 984; *Hanson and Mauersberger*, 1988]. The top diagram indicates the temperature dependence of the $H_2SO_4$ and $HNO_3$ weight percentages. The increase of $w_N$ and decrease of $w_S$ for temperatures falling below the NAT equilibrium temperature is caused by uptake of $H_2O$ and $HNO_3$ [*Carslaw et al.,* 1994].

## Results and Discussion

The polar vortex of winter 1992/93 was characterized by a stable, cold phase lasting from the end of November 1992 to the end of January 1993 [*Naujokat et al.*, 1993]. Despite a temporary vortex split at the end of December 1992 the vortex remained stable leading to low stratospheric temperatures during January.

Figure 2

Results of the size distribution calculations are shown in Figures 2 and 3. Figure 2 gives the temporal development of median particle radius as a function of altitude. Between the tropopause (marked as dashed line) and about 450 K potential temperature we observed the Pinatubo aerosol layer with median radii exceeding 0.3 pm. Above 450 K the temporal variability of $\bar{r}$ increases significantly. The average relative error of $\bar{r}$ is in the order of 60%. Similarly, Figure 3 shows the temporal development of the volume density as a function of altitude. Within the layer of volcanic aerosols volume densities of more than 10 $\mu m^3/cm^3$ are found. The relative errors of $V$ vary between 30 and 50%. We note that at higher altitudes around 480 K volume densities approach almost the background value of 0.1 $\mu m^3/cm^3$ [*Dye et al.*, 1992]. For the graphical representation in Figures 2 and 3 the data sets have been interpolated in time using Gaussian weights with a standard deviation of one day. White areas indicate that either lidar data is not available or values of $\bar{r}$ and $s$ cannot be derived or $\delta_A$ exceeds 0.01.

Figure 3.

As can be seen from Figure 3 volume density $V$ shows a strong temporal variability

Figure 4.

above 450 K during January 1993. Comparison with temperature data obtained from ol]-site balloon soundings (Figure 4) reveals that $V$ increases significantly as $T$ approaches the frost point at all altitude levels between 350 and 550 K. Below 450 K the enhancements are in the order of a factor of two, above 450 K volume changes by one order of magnitude are observed.

Figure 5.

The temperature dependence of $V$ at three altitude levels is shown in Figures 5, 6,

Figure 6.

and 7. The data points in the top diagrams of each figure give geometric means $V(T)$ of

Figure 7.

individual measurements $V(T)$ at altitudes of 400, 440 and 480 K, respectively. While

the layer around 440 K is strongly influenced by the volcanic aerosol with enhanced volume densities (about 2 $\mu m^3/cm^3$), at 480 K background conditions prevail (about 0.1 $\mu m^3/cm^3$) and only very low temperatures lead to the dramatically increased volume densities (up to 30 $\mu m^3/cm^3$) in the course of type Ib PSC formation.

The geometric mean of $\mathcal{V}(T)$ is formed over all data within the temperature interval $[T', T+\Delta T](\Delta T = 0.5$ K) and an altitude interval of $\pm$ 10 K. For each mean value a pair of error bars are presented. The left ones gives the standard deviation of the measurements and the right ones the average error of the individual measurements. Vertical arrows indicate the NAT equilibrium temperature and the frost point. (In the following the NAT equilibrium and frost point temperature are solely used as reference values.)

We note that $V(T)$ is calculated on the basis of 1034 (458, 1 99) measurements with $\delta_A <0.01$ from a total aerosol data set of 1551 (1 092, 508) measurements at 400 K (440 K, 480 K) recorded over a two months period. in calculating the means over data at constant potential temperature we implicitly assume that total $H_2SO_4$ and $HNO_3$ vmr were constant within isentropic layers during December 1992 and January 1993.

This assumption is only partially fulfilled as is indicated in Figure 7 by enhanced values of V at temperatures above 205 1{. Those data sets were recorded on December 24/25 and 31. Trajectory analyses at 4751< indicate that during these days air from lower latitudes were observed above Spitsbergen. Within the polar vortex subsidence in combination with the vertical gradient of total $H_2SO_4$ vmr $x_S$ (cf. Figure 8) leads to a reduction of $x_S$ whereas on these particular days out-of-vortex air led to enhanced values of $x_S$ and therefore larger volume densities were observed. Furthermore, we assume that diabatic vertical transport over more than the width of the chosen altitude interval (20 1{) can be neglected during the measurement period.

At all three altitude levels $V$ increases significantly as temperatures approach the frost point. We compare our observations with results from thermodynamic model

calculations which are in good agreement with available laboratory data [*Carslaw et al., 1994*]. The ST'S model predicts a continuous increase in particle volume as temperatures fall below the NAT equilibrium temperature. The volume increase is caused by the uptake of $H_2O$ and $HNO_3$ into the liquid aerosol due to the enhanced solubility of these gases at low temperatures. The analytic expressions given by *Carslaw et al. [1*995] which represent a simplified formulation of the thermodynamic STS model are used here to determine particle volume and composition. The model yields particle composition in terms of the $H_2SO_4$ and $HNO_3$ weight percentages and the volume density as a function of temperature, atmospheric pressure, ambient $H_2O$ vmr and $H_2SO_4/HNO_3$ molar concentrations. Mass conservation of $HNO_3$ is taken into account.

The model results are given as solid line in the top diagrams of Figures 5, 6, ant] 7. '1'eta] $H_2SO_4$ vmr is determined with a least square fit. The result for twice (half) the amount of $x_s$ is shown by the dashed (das])cd-dotted) line. Additionally, the temperature dependence of $H_2SO_4$ and $HNO_3$ weight percentages as derived from the S'1'S model is plotted in the center diagrams of Figures 5, 6, ant] 7, respectively. The bottom diagrams indicate the $HNO_3$ gas phase depletion in terms of the ratio of $HNO_3$ vmr and $HNO_3$ total vmr.

The good agreement between observed and calculated volume densities at all three altitude levels suggests that the observed aerosols between 350 and 550 K are composed of (; liquid ternary solutions of sulfuric and nitric acid. Therefore, we believe that volcanic aerosols at low temperatures and type 1 b PSC should be considered to belong to the same class of stratospheric aerosols. The apparent lack of a discontinuity in $V(T)$ at the NAT equilibrium temperature indicates that the composition of these low-depolarization particles is not NAT. At all three altitude levels considerable $HNO_3$ gas phase depletion of more than 90% should accompany particle growth at temperatures close to the frost point. This could have considerable consequences for the formation probability of NAT particles since the NAT equilibrium temperature drops by 3.2 K

if 10 ppbv $HNO_3$ gas phase vmr at 50 hPa altitude is reduced to 1 ppbv assuming
5 ppmv $H_2O$ [*Hanson and Mauersberger, 1988*].

our comparison of observed and calculated aerosol volume densities allows us to estimate an altitude profile of total $H_2SO_4$ vmr. For all altitude levels between 350 and 500 K with a step size of 10 K we fitted the total $H_2SO_4$ vmr for the calculated volume densities to agree with the observations. The result together with the value of $\chi^2$ is shown in Figure 8. Total $H_2SO_4$ volume mixing ratios decrease from 4 ppbv at 350 K to less than 0.5 ppbv above 450 K. The low values above about 450 K are consistent with background levels of stratospheric aerosols [*Dye et al.*, 1992].

## Conclusion

Arctic lidar measurements during the vole.a~lically perturbed winter 1992/93 are analyzed. Volume densities of stratospheric aerosols with aerosol depolarization less than 0.01 were found to decrease from about 10 $\mu m^3/cm^3$ at 350 K to near Background values of 0.1 $\mu m^3/cm^3$ above 500 K potential temperature. At all altitude levels between 350 and 5.50 K a 2- to 30 fold increase in particle volume was observed as temperatures approached the frost point.

The good agreement between observed and calculated volume densities leads us to the following conclusions.

- The smooth dependence of V on temperature indicates that both the volcanic sulfuric acid aerosol and the background sulfuric aerosol were not frozen but in the liquid state. This result is consistent with model calculations [*Luo et al.*, 1994].

- The apparent lack of a sharp increase in $V(T)$ just below the NAT equilibrium temperature indicates that the particle composition is not NAT.

- Comparison between observed volume densities at all three altitude levels and model results suggests that the observed aerosols between 350 and 550 K with

$\delta_A < 0.01$ are composed of a ternary solution of sulfuric and nitric acid.

- Considerable $HNO_3$ gas phase depletion of more than 90% occurs at all three altitude levels for temperatures close to the frost point reducing the probability of NAT particle formation.

However, more than 3570 of the total aerosol data set shows aerosol depolarization of more than 0.01 indicating the presence of non-spherical particles. The composition of these solid PSC type la particles is still unclear.

# References

Beyerle, G'., and R. Neuber, The stratospheric aerosol content above Spitsbergen during winter 1991/92, *Geophys. Res. Lett.*, *21*, (13), 1291-1294, 1994.

Beyerle, G., R. Neuber, O. Schrems, F. Wittrock, and B. Knudsen, Multiwavelength lidar measurements of' stratospheric aerosols above Spitsbergen during winter 1 992/93, *Geophys. Res. Lett.*, *21*, (1), 57-60, 1 994.

Bohren, c. F., and D. R. Huffman, *A bsorption and scattering of light by small particles*, John Wiley & Sons, New York, 1983.

Browell, E. V., C. F. Butler, S. Ismail, P. A. Robinette, A. F. Carter, N. S. Higdon, O. B. Toon, M. R. Schoeberl, and A. F. Tuck, Airborne lidar observations in the wintertime Arctic stratosphere: Polar stratospheric clouds, *Geophys. Res. Lett.*, *19*, (9), 385 388, 1990.

Carslaw, K. S., B. P. Luo, S. L. Clegg, T. Peter, 1'. Brimblecombe, and P. J. Crutzen, Stratospheric aerosol growth and $HNO_3$ gas phase depletion from coupled $HNO_3$ and water uptake by liquid particles, *Geophys. Res. Lett.*, *21*, (23), 2479 2482, 1994.

Carslaw, K. S., B. 1'. Luo, and T. Peter, An analytic expression for the composition of aqueous $HNO_3$-$H_2SO_4$ stratospheric aerosols including gas phase removal of $HNO_3$, *Geophys. Res. Lett.*, 22, (14), 1877- 1880, 1995.

Deshler, T., In situ measurements of Pinatubo aerosol over Kiruna on four days between 18 January and 13 February 1992, *Geophys. Res. Lett.*, *21*, (1 3), 13231326, 1994.

Drdla, K., A. Tabazadeh, R. 1'. Turco, M. Z. Jacobson, J. E. Dye, C. Twohy, and D. Baumgardner, Analysis of the physical state of one arctic. polar stratospheric cloud based on observations, *Geophys. Res. Lett.*, *21*, *(23), 2475-2478,* 1994.

Dyc, J. E., 1). Baumgardner, B. W. Gandrud, S. R. Kawa, K. K. Kelly, M. Loewenstein, G. V. Ferry, K. R. Chan, and B. L. Gary, Particle size distributions in Arctic polar stratospheric clouds, growth and freezing of sulfuric acid droplets, and implications for cloud formation, *J. Geophys. Res.*, *97*, (D8), *8015-8034, 1992*.

Gille, J. C., and J. M. Russell, The limb infrared monitor of the stratosphere: Experiment description, performance, and results, *J. Geophys. Res.*, *89*, *(1)4)*, 5125 *5140, 1984*.

Hanson, D., and K. Mauersberger, laboratory studies of the nitric acid trihydrate: Implications for the south polar stratosphere, *Geophys. Res. Lett.*, *15*, (8), 855 858, 1988.

Heintzenberg, J., H. Müller, ]]. Quentzel, and E. Thomalla, Information content of optical data with respect to aerosol properties: numerical studies with a randomized minimization- scare}]- technique inversion algorithm, *Appl. Opt.*, *20*, *(8)*, 1308 1315, 1981.

Jäger, 11., and D. Hofmann, Midlatitude lidar backscatter to mass, area, and extinction conversion model based on in situ aerosol measurements from 1980 to 1987, *Appl. Opt.*, *30*, *(1)*, *127-138, 1991*.

Klett, J. D., Lidar inversion with variable backscatter/extinction ratios, *Appl. Opt.*, *24*, (11), 1638-1643, 1985.

1<00]), T., U. M. Biermann, W. Raber, B. P. Luo, P. J. Crutzen, and T. Peter, Do stratospheric aerosol droplets freeze above the ice frost point?, *Geophys. Res. Lett.*, 22, (8), 917-920, 1995.

Larsen, N., Stratospheric aerosols, backscatter measurements from Thule, European Arctic Stratospheric Ozone Experiment, Report 92-1, Danish Meteorological Institute, 1992.

Luo, B. P., T. Peter, and P. J. Crutzen, Freezing of stratospheric aerosol droplets, *Geophys.Res.Lett.,21*, (] 3), 1447-1450, 1994.

McCormick, P. M., and R. E. Veiga, SAGE II measurements of early Pinatubo aerosols, *Geophys. Res. Lett.,19*, (2), ] 55- ] 58, ] 992.

Meilinger, S., T. Koop, B. Luo, T. Huthwelker, 1{. S. Carslaw, U. Krieger, 1'. J. Crutzen, and T. Peter, Size-dependent stratospheric droplet composition in mesoscale temperature fluctuations and their potential role in PSC freezing, *Geophys. Res. Lett., 22,3031-3034, 1995.*

Naujokat, B., K. Petzoldt, K. Labitzke, R. Lenschow, B. Rajewski, M. Wiesner, and R.-C. Wohlfart, The stratospheric winter 1992/93: A cold winter with a minor warming and a late final warming, *Beilage zur Berliner Wetterkarte,* 1993.

Neuber, R., G. Beyerle, and (). Schrems, LIDAR measurements of stratospheric aerosols in the Arctic, *Ber. Bunsenges.Phys.Chem.,96, (3), 350 353, 1992.*

Ovarlez, J., and H. Ovarlez, Stratospheric water vapor content evolution during EASOE, *Geophys.Res.Lett.,* 21, (1 3), 1235 1238, 1994.

'almer, K. F., and D. Williams, Optical constants of sulfuric acid; Application to the clouds of Venus?, *Appl.Opt.,14,(1 ),* 208 219, 1975.

'innick, R. G., J. M. Rosen, and D. J. Hofmann, Stratospheric aerosol measurements III: Optical model calculations, *J. Atmos. Sci.,* 33, 304- 3]4, 1976.

Poole, L. R., and M. 1'. McCormick, Airborne lidar observation of arctic polar stratospheric clouds, *Geophys. Res. Lett.,15*, (1), 2]- 23, 1988.

Russell, 1'. 11., and 1'. Hamill, Spatial variation of stratospheric aerosol acidity and model refractive index: Implications of recent results, *J. Atmos. Sci., 41*, (11 **),** *1781-1790, 1984.*

Steele, H. M., and P. Hamill, Effects of temperature and humidity on the growth and optical properties of sulphuric acid-water droplets in the stratosphere, *J. Aerosol Sci.*, *12*, **(6)**, *517-.528, 1981.*

Tabazadeh, A., R. P. Turco, and M. Z. Jacobson, A model for studying the composition and chemical effects of stratospheric aerosols, *J. Geophys. Res.*, *99*, ( 1 ) 6 ) , 12897-12914, 1994.

Thomalla, E., and 11. Quenzel, Information content of aerosol optical properties with respect to their size distribution]], *Appl. Opt.*, *21*, (17), 31703177, 1982.

Thomason, L. W., and M. T. Osborn, Lidar conversion parameters derived from SAGE 11 extinction measurements, *Geophys. Res. Lett.*, *19*, (16), 1655 1658, 1992.

Toon, (). B., E. V. Browell, S. Kinne, and J. Jordan, An analysis of lidar observations of polar stratospheric clouds, *Geophys. Res. Lett.*, *17*, (4), 393 396, 1990.

Toon, O. B., E. Browell, B. Gary, L. Lait, J. Livingston, 1'. Newman, R. Pueschel, 1'. Russell, M. Schoeberl, G. Goon, W. Traub, F. 1'. J. Valero, 11. Selkirk, and J. Jordan, Heterogeneous reaction probabilities, solubilities, and the physical state of cold volcanic aerosols, *Science*, *261*, 1136 1140, 1993.
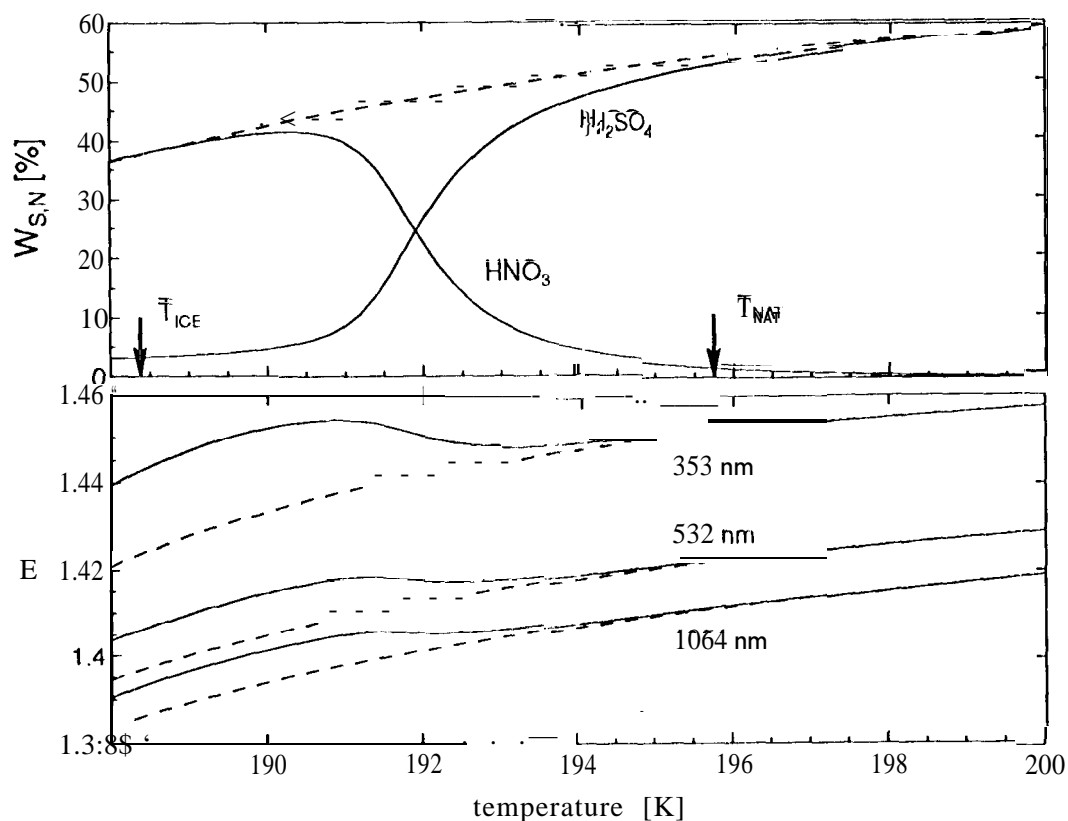
# Figure Captions



**Figure 1. Top:** $HNO_3$ and $H_2SO_4$ weight percentages at 50 mbar altitude (solid lines: ternary, dashed line: binary system). Assumed total vmr of $H_2O$, $HNO_3$ and $H_2SO_4$ are 5 ppmv, 10 ppbv and 0.5 ppbv, respectively. The vertical arrows indicate the NAT equilibrium temperature and frost point. Bottom: temperature dependence of refractive indices at *353, 532* and 1064 nm (solid: ternary, dashed: binary).
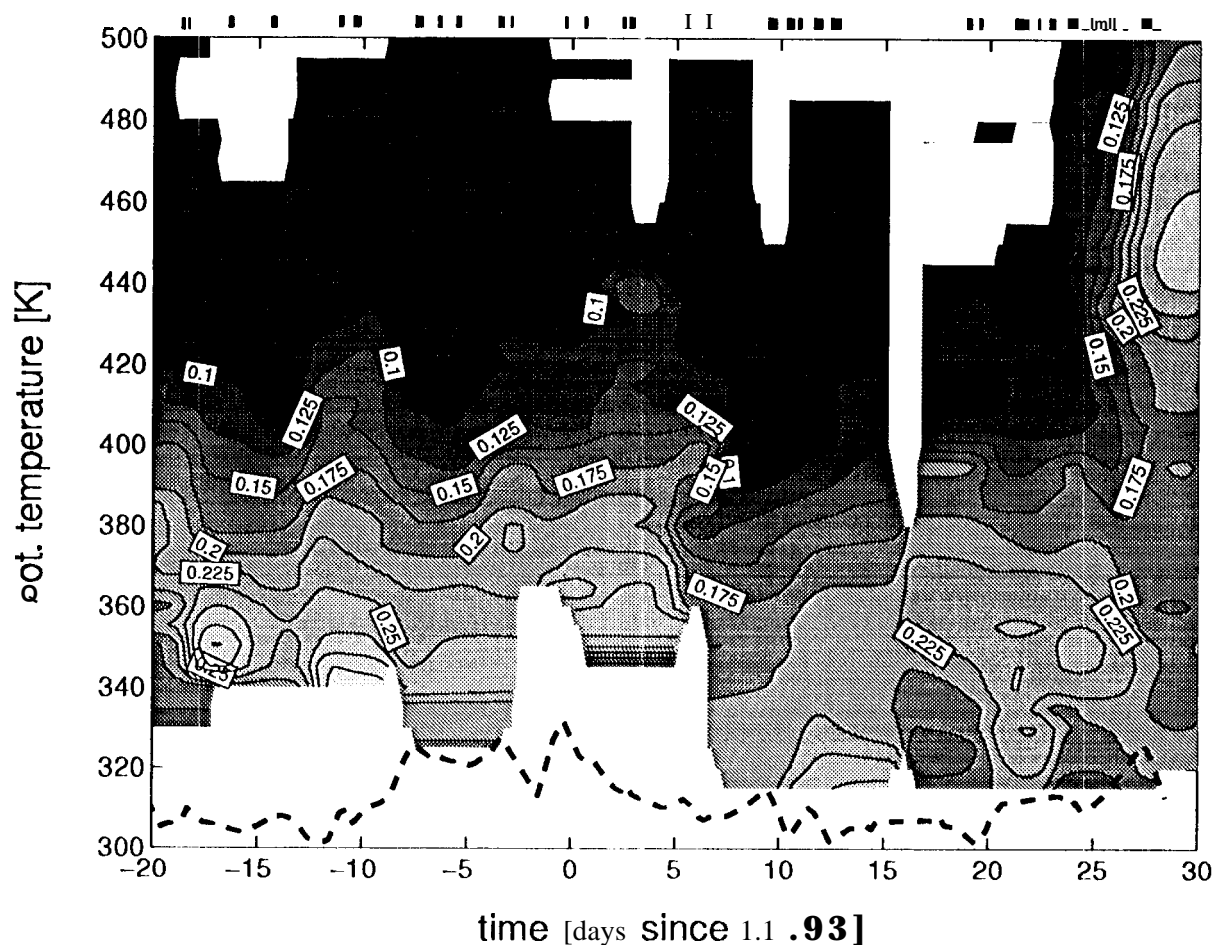
Figure 2. Temporal development of median radius $\bar{r}$ as a function of potential temperature during winter 1992/93. $\bar{r}$ is shown in units of $\mu$m. The dashed line gives the tropopause altitude. Bars above the figure indicate the time of the individual measurements. White areas indicate that either lidar data is not available or values of $\bar{r}$ and $s$ cannot be derived or $\delta_A$ exceeds 0.01.
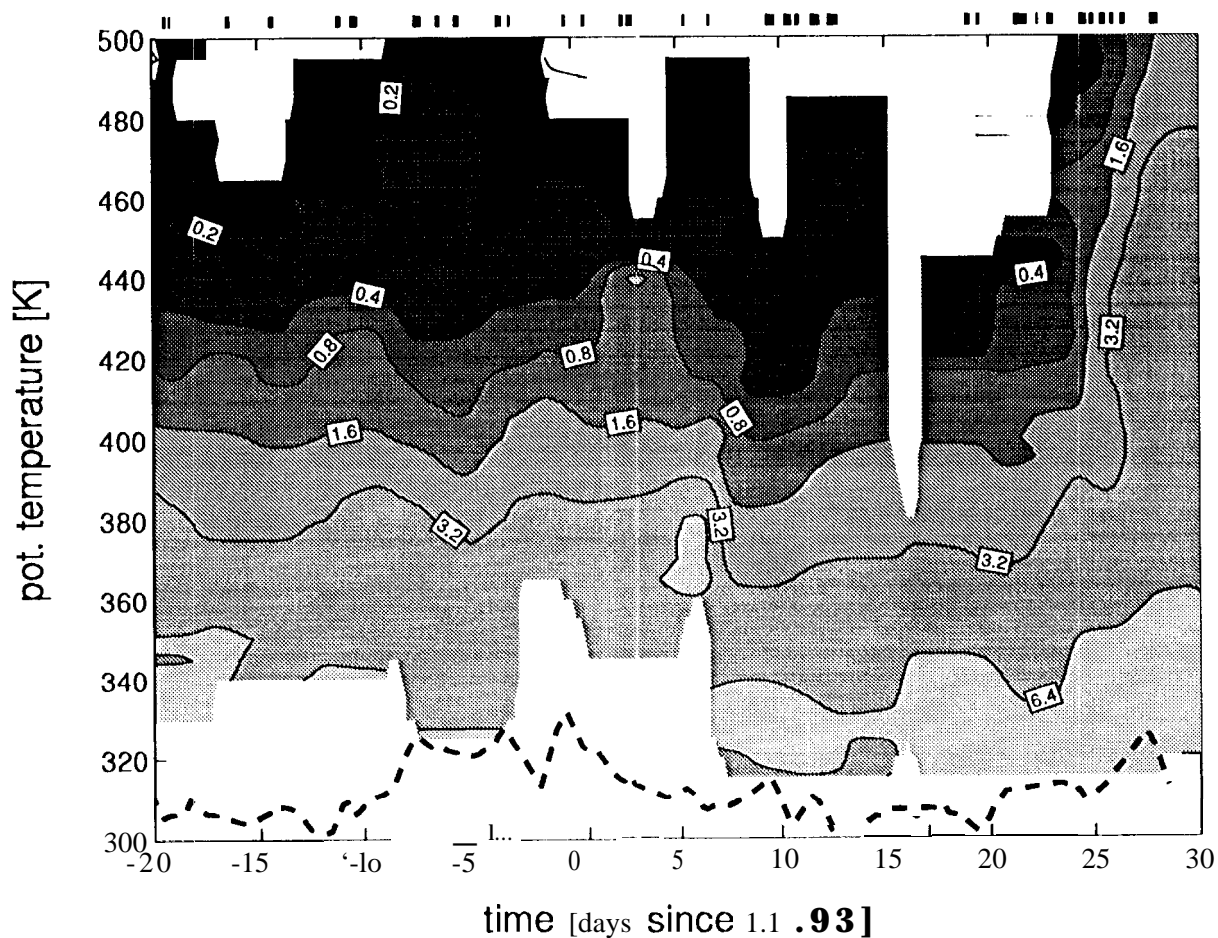
**Figure 3.** Temporal development of volume density $\mathcal{V}$ as a function of potential temperature during winter 1992/93. $\mathcal{V}$ is shown in units of $\mu m^3/cm^3$.
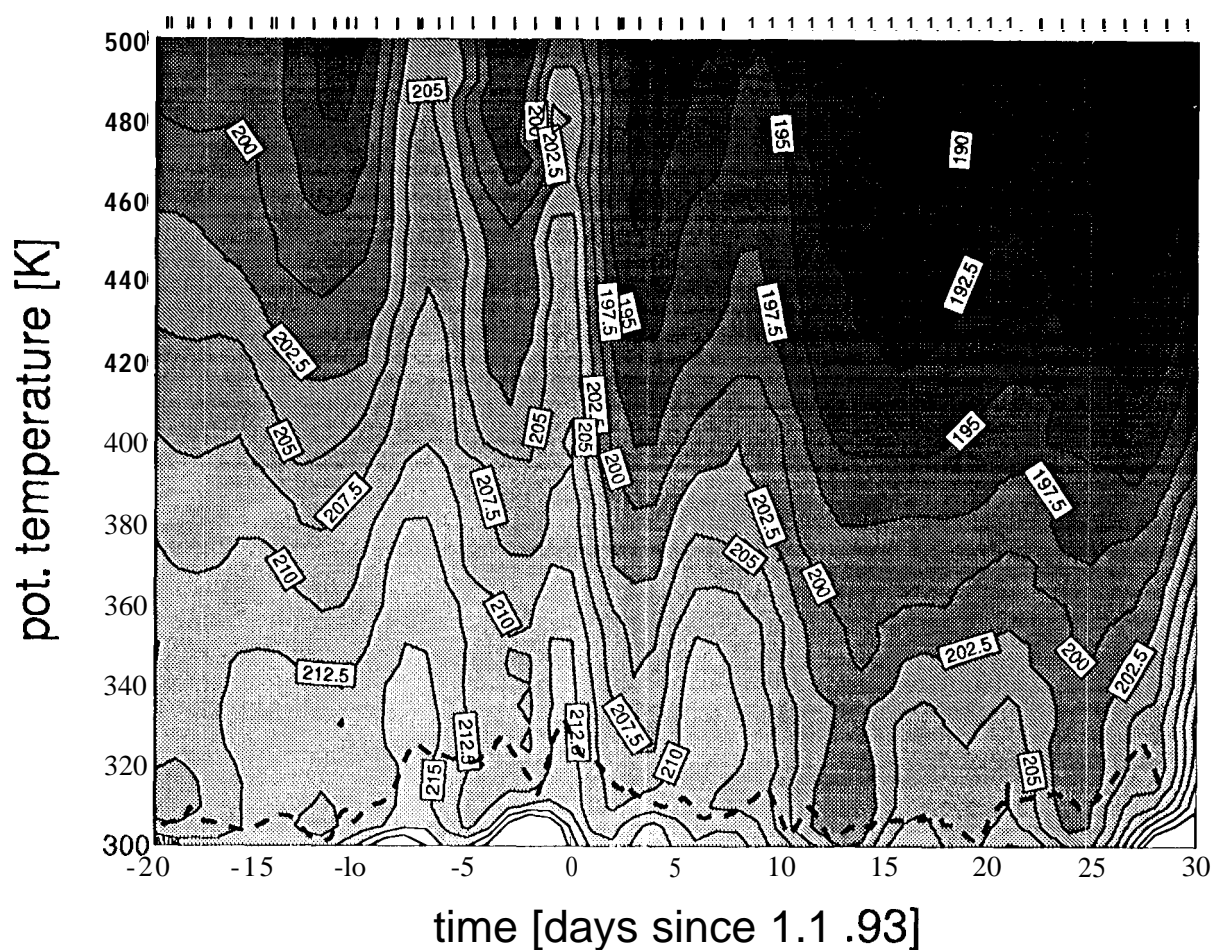
**Figure 4.** Temporal development of atmospheric temperature $T$ as a function of potential temperature during winter 1992/93 derived from daily aerological soundings at Ny-Ålesund. $T$ is shown in units of K.
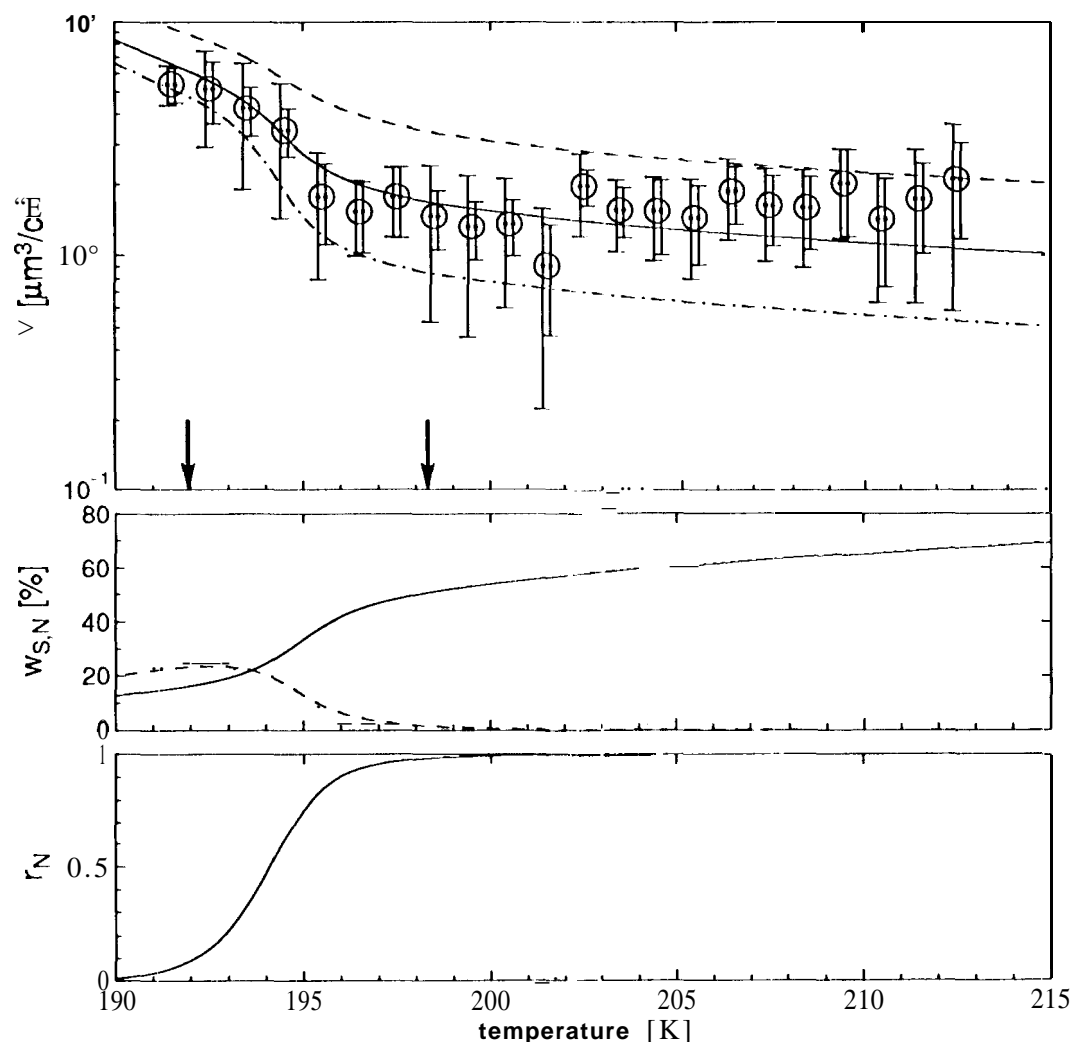
**Figure 5.** Temperature dependence of volume density at the 40( 1 K isentropic level (top). $HNO_3$ and $H_2O$ vmr are assumed to be 5.7 ppbv (1,] MS) and 5 ppmv, respectively. The data points are geometric mean values of measurements recorded over a period of two months. Mean atmospheric pressure is $91\pm 11$ hPa. Results from S'1'S model calculation) are shown as solid line where total $H_2SO_4$ vmr of 2.3 ppbv is derived from a least square fit to the data. The dashed (clashed-dotted) line gives the volume density for twice (half) the amount of total $H_2SO_4$ vmr. Arrows indicate the NAT equilibrium temperature and the frost point. The center diagram shows the temperature dependence of $HNO_3$ (dashed line) and $H_2SO_4$ (solid line) weight percentages. The $HNO_3$ gas phase fraction ($HNO_3$ vmr/ $HNO_3$ tots] vmr) as a function of temperature is given in the bottom diagram.
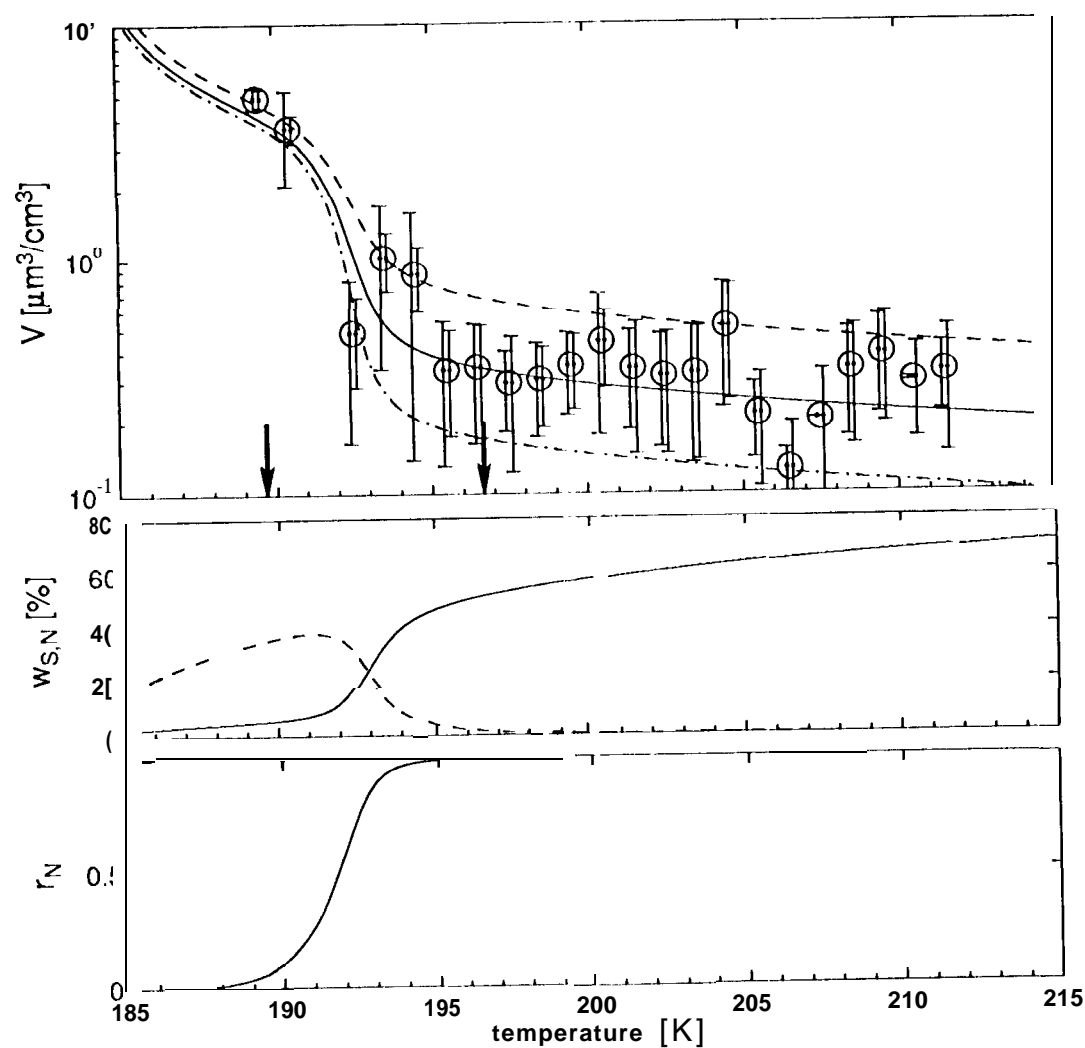
Figure 6. The same as Figure 5, however for an altitude of 440 K potential temperature. $HNO_3$ and $H_2O$ vmr are assumed to be 7.9 ppbv (LIMS) and 5 ppmv, respectively. Mean atmospheric pressure is 63±7.9 hPa. The least square fit yields a total $H_2SO_4$ vmr of 0.69 ppbv.
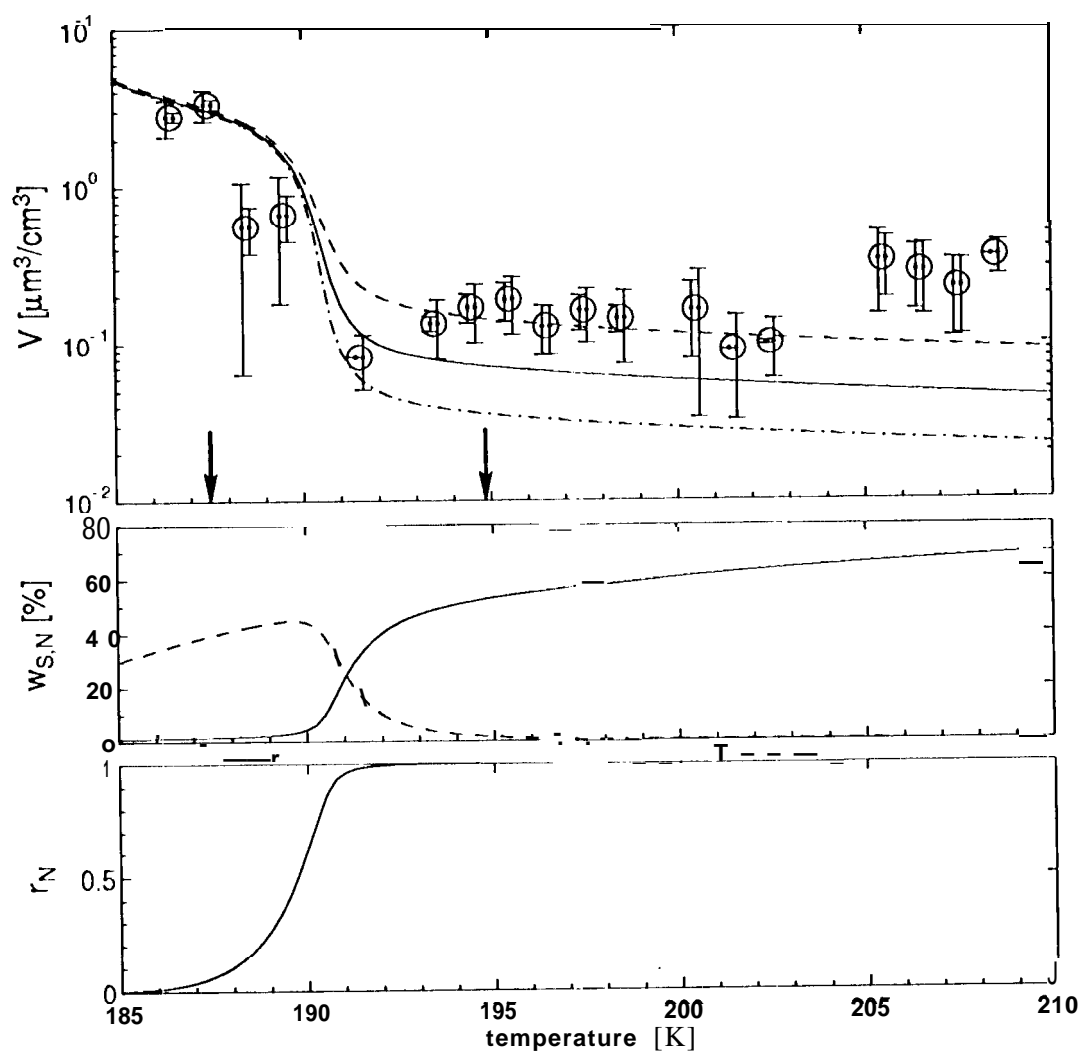
**Figure.** 7. The same as Figure 5, however for an altitude of 480 K potential temperature. $HNO_3$ and $H_2O$ vmr are assumed to be 9.6 ppbv (LIMS) and 5 ppmv, respectively. Mean atmospheric pressure is $43 \pm 6.6$ hPa. The least square fit yields a total $H_2SO_4$ vmr of 0.22 ppbv.
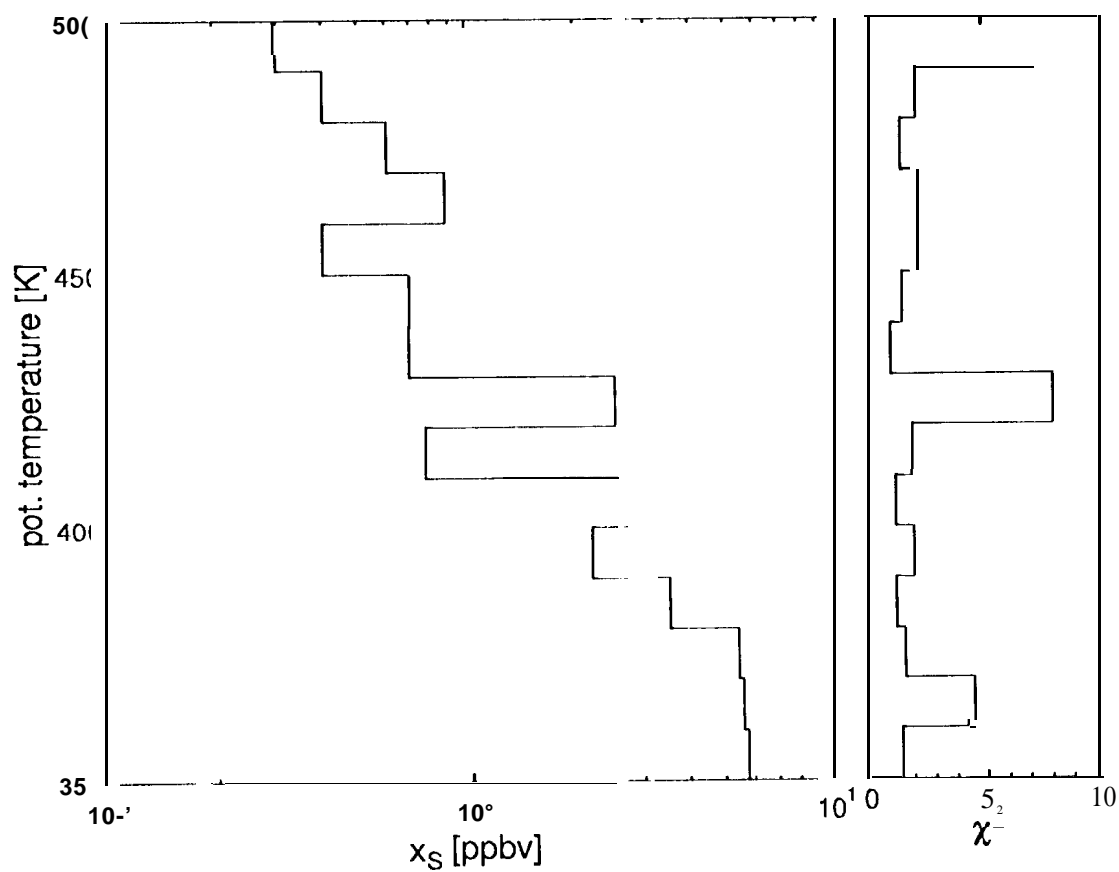
**Figure** 8. Total $H_2SO_4$ volume mixing ratio $(x_S)$ as a function of altitude derived from the comparison between S'1'S model and observation (left). On the right hand side $\chi^2$ of the fit is shown.